Tunable Electrical Properties of Ti-B-N Thin Films Sputter-Deposited by the Reactive Gas Pulsing Process

Charalampos Sakkas, Jean-Marc Cote, Joseph Gavoille, Jean-Yves Rauch, Pierre-Henri Cornuault, Anna Krystianiak, Olivier Heintz, Nicolas Martin

coatings

Article

Tunable electrical properties of Ti-B-N thin films sputter-deposited by the reactive gas pulsing process

Charalampos Sakkas [1], Jean-Marc Cote [1], Joseph Gavoille [1], Jean-Yves Rauch [1], Pierre-Henri Cornuault [1], Anna Krystianiak [2], Olivier Heintz [2] and Nicolas Martin [1,*]

[1] Institut FEMTO-ST, UMR 6174, CNRS, ENSMM, Univ. Bourgogne Franche-Comté, 15B, Avenue des Montboucons, 25030 BESANCON Cedex, France
[2] Laboratoire Interdisciplinaire Carnot de Bourgogne (ICB), UMR 6303, CNRS, Univ. Bourgogne Franche-Comté, 9, Avenue Alain Savary, BP 47 870, F-21078 DIJON Cedex, France
* Correspondence: nicolas.martin@femto-st.fr; Tel.: +33-363-08-2431

Abstract: Titanium-boron-nitrogen (Ti-B-N) thin films were deposited by RF reactive magnetron sputtering using a titanium diboride (TiB_2) target in an argon + nitrogen mixture. The argon mass flow rate was kept constant whereas that of nitrogen was pulsed during the deposition. A constant pulsing period P = 10 s was used and the introduction time of the nitrogen gas (duty cycle dc) was systematically varied from dc = 0 to 100% of the pulsing period. This reactive gas pulsing process allowed depositing Ti-B-N thin films with various boron and nitrogen concentrations. Such adjustable concentrations in the films also led to changes of their electronic transport properties. Boron and nitrogen contents exhibited a reverse evolution as a function of the nitrogen duty cycle which was correlated with the transition from a metallic-to-semiconducting-like behavior. A percolation model was applied to the electrical conductivity as a function of the nitrogen pulsing parameters assuming some correlations with the evolution of the Ti-B-N thin films nanostructure.

Keywords: Ti-B-N; reactive sputtering; gas pulsing; electrical conductivity; percolation.

Citation: Sakkas, C.; Cote, J.M.; Gavoille, J.; Rauch, J.Y.; Cornuault, P.H.; Krystianiac, A.; Heintz, O.; Martin, N. Tunable electrical properties of Ti-B-N thin films sputter-deposited by the reactive gas pulsing process. *Coatings* **2022**, *12*, 1711. https://doi.org/10.3390/coatings12111711

1. Introduction

The development of nanostructured thin films by reactive sputtering for a wide range of applications has nowadays become one of the challenging tasks for creating innovative functional materials. If binary compounds combining two metallic elements, or a single metal with a light element such as carbon, boron, nitrogen or oxygen, have been extensively investigated for these last decades, the addition of a third element to form ternary materials still remains relevant today since the association of three elements may lead to the formation of one, two or even multi-phase systems and so nanocomposite materials [1-3]. As a result, one of the most interesting features of these multiphasic materials is that their properties can be tailored by playing with the size, volume fraction, distribution, composition and so on of the appropriate phases. Among the large family of ternary compounds, many investigations have been focused on combinations of two metals with a light and reactive element [4-8]. It is quite common to associate two metals with nitrogen or carbon for hard coatings [9, 10], or with oxygen for optical applications [11, 12]. Other studies report on metallic oxynitrides MO_xN_y, oxycarbides MO_xC_y or carbonitrides MN_xC_y from one metal with the two corresponding elements (i.e., oxygen + nitrogen, oxygen + carbon, or nitrogen + carbon, respectively) [13-17]. For these last thin film materials, one of the challenging tasks is the high reactivity of light elements towards the sputtered metal, which may restrain some reachable compositions and, thus limiting the range of final properties.

Among ternary compounds, the ternary metal boron nitrides, namely M-B-N, have been compiled by Rogl [18] for several metals. Such experimental data show that the phase

diagram feature strongly depends on the metal affinity towards boron and nitrogen and these ternary systems can be classified with respect to the chemical ability of the metal element to form or not binary borides, binary nitrides and/or ternary boron nitride compounds. Furthermore, consistent with this compilation, most relevant works devoted to metal boron nitride thin films systematically claim about the key role played by the nitrogen incorporation during the processing stage. This is particularly true when metal boron nitride films are prepared by reactive sputtering where the control of the process (and so the resulting film properties) strongly depends on the nitrogen partial pressure [19-22]. Titanium boron nitrides Ti-B-N are no exception and phase mixture consisting of materials with different properties can be produced [23-25]. Since hard phases such as TiN, TiB_2, and cubic BN may coexist with soft phases such as hexagonal BN or amorphous BN, the very large majority of studies about Ti-B-N films have been focused on their mechanical and tribological properties as hard and wear-resistant coatings [26-29]. It is also worth noting that enhanced hardness and good wear resistance of Ti-B-N thin films sputter-deposited have been accordingly connected to the produced nanocomposite structure; the latter being closely related to the film composition and thus dependent on the nitrogen partial pressure implemented during the deposition process.

Although there are many investigations on understanding mechanical performances of Ti-B-N films, very little work has been performed on their electrical behaviors as a function of B and N contents. It is particularly interesting to know how electronic transport properties change as a function of B and N concentrations since pure TiB_2 and TiN materials both exhibit metallic-like behaviors. Combining these two materials often showed optimized mechanical and tribological properties for some given amounts of TiB_2 and TiN in an amorphous matrix of BN. Since BN is an insulating material and assuming a nanocomposite structure of Ti-B-N films, the motivation of this article is to understand how the electrical conductivity of Ti-B-N films can be tuned *vs*. light elements concentration, and to determine some correlations with the most relevant sputtering process parameters.

In this work, we prepared Ti-B-N thin films by reactive sputtering using the reactive gas pulsing process (RGPP) [30]. Nitrogen mass flow rate is periodically supplied during the deposition stage with an increasing time of injection. The chemical composition is first determined so as to prove that B and N contents are adjustable by means of nitrogen gas pulsing. Electrical properties (resistivity, charge carrier mobility and concentration) are systematically measured and illustrate significant variations of Ti-B-N films conductivity for some given nitrogen pulsing parameters, and so as the nitrogen concentration in the films increases. Assuming a nanocomposite structure of Ti-B-N films, a percolation model is suggested to explain their electronic transport properties.

2. Materials and Methods

Ti-B-N thin films were prepared by RF reactive magnetron sputtering. The sputtering machine was a 110 L vacuum chamber evacuated by a cryogenic pump backed with a dry primary pump achieving an ultimate pressure of 5×10^{-8} mbar. A TiB_2 rectangular target (381×127×6.35 mm and purity 99.9%) was fixed at 100 mm from the centre of the substrate holder. The argon flow rate was kept constant at q_{Ar} = 29 sccm and a constant pumping speed S_{Ar} = 95 L s^{-1} was used, leading to an argon partial pressure of 0.6 Pa. Before any deposition, an etching period of 15 min and 250 V of bias was applied to the substrates. Then, the TiB_2 target was RF sputtered using a constant electric power of 1 kW. Furthermore, a pre-sputtering time was applied for 5 min to remove the contamination layer on the target surface and stabilize the process, leading to a target self-bias potential of V_{SB} = 210 V. Nitrogen flow rate q_{N2} was pulsed during Ti-B-N deposition by means of the RGPP [30]. A rectangular signal was used to pulse nitrogen gas with a constant pulsing period P = 10 s. This period was selected since such operating conditions correspond to a freedom of alternating between the boride and nitride poisoned state and vice-versa. For all depositions the nitrogen injection time t_{ON} was varied, from 0 to 10 s, corresponding to

duty cycles *dc* (*dc* = t_{ON}/P) from 0 until 100% of *P*. The maximum nitrogen rate was q_{N2Max} = 5 sccm. This value corresponds to the nitrogen amount required to completely avalanche the reactive sputtering process in the nitride sputtering mode [31]. During the t_{OFF} time, the nitrogen mass flow rate was completely stopped (q_{N2min} = 0 sccm). The total sputtering pressure and TiB_2 target voltage were alternated in the range of 6.0–6.3×10^{-3} mbar and 210–220 V for t_{OFF} and t_{ON} times, respectively. During deposition, the substrate holder (191×142 mm) was biased with a negative voltage of 20 V, and no external heating was added. Ti-B-N films were deposited on glass and (100) Si substrates. Deposition rate was measured from the film thickness and the corresponding deposition time. The latter was adjusted in order to get a constant film thickness of 300 nm.

Electrical resistivity measurements, from room temperature (25° C) until 200° C, were conducted with a homemade system using the four-probe van der Pauw method, equipped with an annealing hot plate. Carriers' concentration and carriers' mobility were assessed from setup when applying a magnetic field B = 0.8 T in a device again operating with the van der Pauw method. The infrared analysis was performed with a Perkin Elmer Spectrum Two Lita FT-IR spectrometer for the range of wavenumbers 400 until 4000 cm^{-1}. The film composition was obtained by X-ray photoelectron spectroscopy (XPS) with a PHI VersaProbe 1 system using a monochromatized and focalized Al Kα X-ray source ($h\upsilon$ = 1486.7 eV, spot diameter = 200 micrometers). Base pressure during analysis is better than 5.10^{-7} Pa. CasaXPS software is used for data treatment [32].

3. Results

The deposition rate *R* of Ti-B-N films was first measured as function of the nitrogen duty cycle *dc* (Fig. 1). It was obtained from thickness measurements of the films (average of 10 measurements giving rise to error bars of the deposition rate) by mechanical profilometry (step height method) and recording the time of deposition.

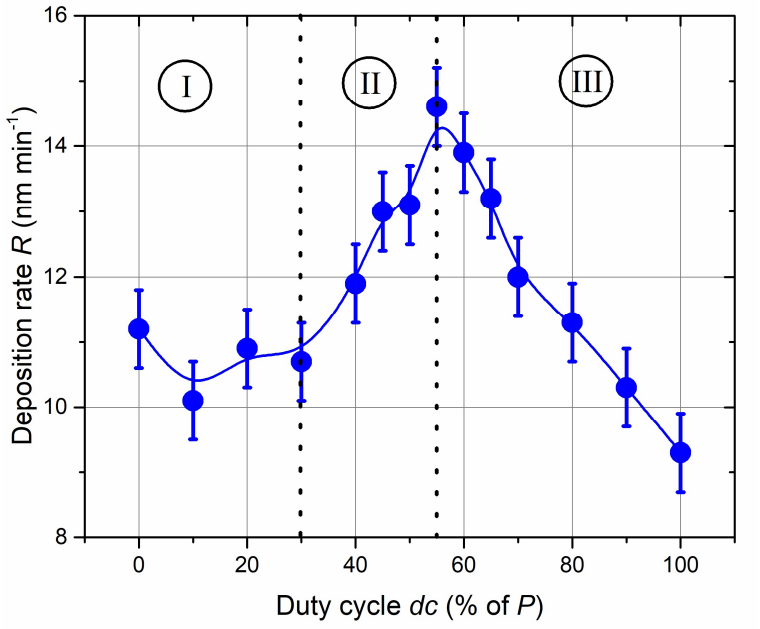

Figure 1. Ti-B-N deposition rate *R* as a function of the duty cycle *dc* when a TiB_2 target is RF sputtered and injecting the nitrogen gas with a pulsing period *P* = 10 s. Deposition rate gradually changes and exhibits a maximum for *dc* close to 55% of *P*.

The evolution of deposition rate *vs.* duty cycle can be divided in three regions (I, II and III in Fig. 1). For duty cycles lower than 30% of *P* (region I) a nearly constant rate can be assumed. Nitrogen injection time (less than 30% of *P* = 10 s) is too short for a full nitriding of the TiB_2 target surface. The boride sputtering mode prevails and one can

expect Ti-B-N films exhibiting characteristics similar to the TiB_2 compound, i.e., a metallic-like behavior. An increase of duty cycle from 30% to 55% of the pulsing period *P* (region II) gives rise to enhanced deposition rates from 10.7 to 14.6 nm min^{-1}, respectively. Deposition rate exhibits a maximum for *dc* = 55% of *P* and a further increase of duty cycle (region III) produces a continuous and linear drop of the deposition rate down to 9.3 nm min^{-1} when the nitrogen gas is constantly supplied (i.e., for *dc* = 100% of *P*. For duty cycles lower than 55% of *P*, the nitrogen injection time (t_{ON} time) is too short to completely set the reactive sputtering process in the nitride mode. Alternations between nitride and boride modes occur during t_{ON} and t_{OFF} times, respectively. Nitride mode prevails for duty cycles higher than 55% of *P* and the TiB_2 target surface becomes more and more covered by a nitride compound, which reduces the sputtering yield. Similarly, there is a progressive incorporation of nitrogen atoms into the Ti-B-N films as the nitrogen injection t_{ON} time is increased corresponding to the formation of a poisoning nitride layer on the target surface and a decrease of the deposition rate. This optimized deposition rate *vs.* nitrogen injection corroborates with results previously reported by Chaleix and Machet [33] and later by Pierson *et al.* [34] where a maximum rate was also obtained for a given range of nitrogen flow rates. In like manner, the authors assigned this maximum rate to a nitrogen incorporation into the growing films and a progressive nitriding of the target leading to a decrease of the deposition rate (typical of low reactive systems).

3.1. Composition and structure

The films composition as a function of the duty cycle is first determined from XPS analyses. XPS spectra show clear signals corresponding to Ti 2p, N 1s and B 1s peaks. (Fig. 2).

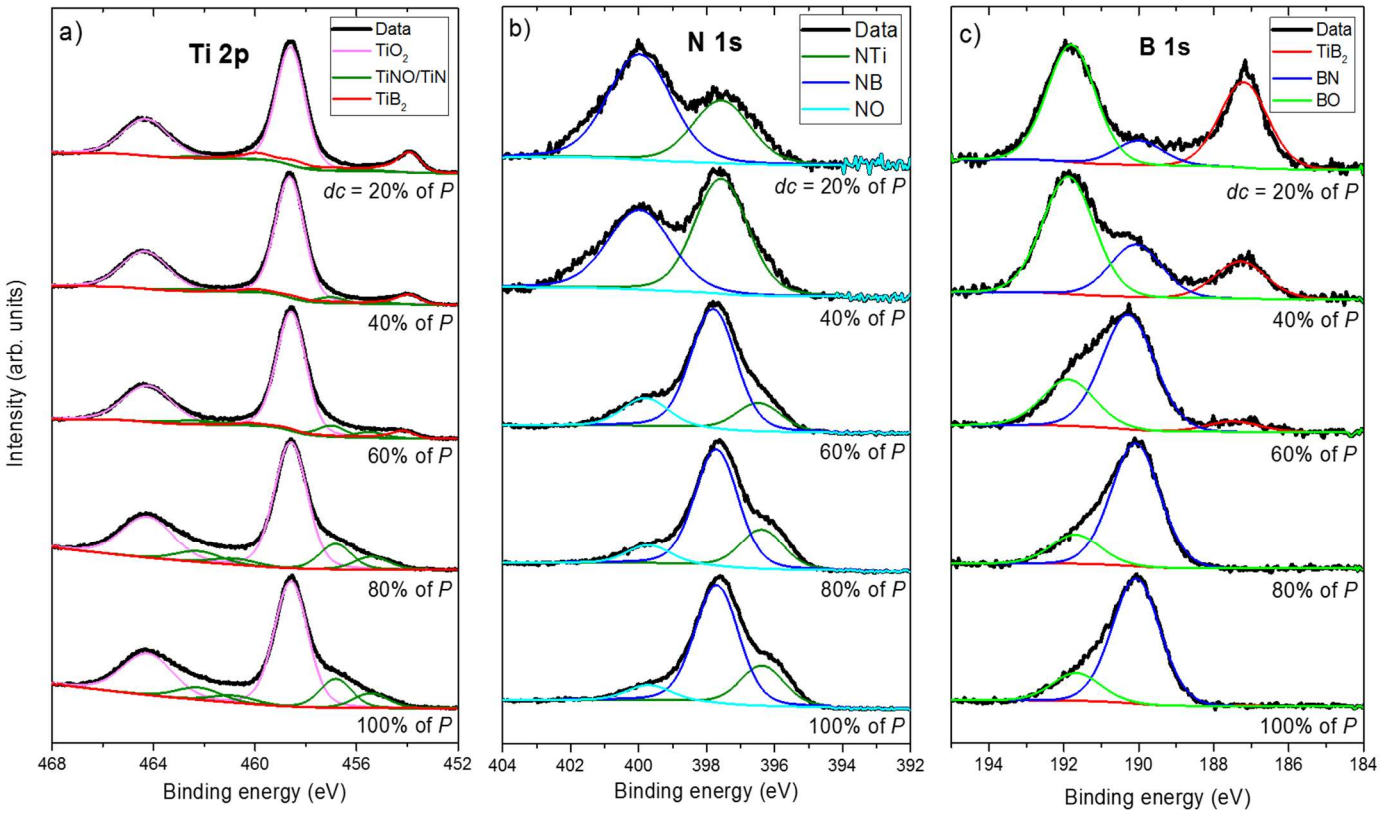

Figure 2. XPS a) Ti 2p, b) N 1s and c) B 1s spectra of Ti-B-N thin films prepared with various duty cycles *dc*.

The position of these peaks agrees with results recorded by other investigators [35, 36]. A curve fitting procedure has been systematically performed for all recorded signals and for various duty cycles. Ti 2p peak consists of three components corresponding to the

contributions from TiO_2 (458.2 and 464.1 eV due to Ti $2p^{1/2}$ and Ti $2p^{3/2}$, respectively), TiNO/TiN (456.7 and 462.3 eV) and TiB_2 (454.3 eV), as illustrated in Fig. 2a. For N 1s spectra (Fig. 2b), decomposition leads to three contributions: NTi (396.9 eV), NB (398.3 eV) and NO (402.8 eV). B 1s spectra also display three contributions assigned to TiB_2 (187.8 eV), BN (190.0 eV) and BO (192.1 eV).

For the 2p levels of titanium (Fig. 2a), the decomposition is more complicated. The contributions of TiO_2 are still visible at 458.2 and 464.1 eV due to Ti $2p^{1/2}$ and Ti $2p^{3/2}$, respectively. The main difficult issue remains determining the contributions of TiN/TiNO on one hand and TiB_2 on the other hand. For each of these compounds, the forms are complex and cannot be reduced to a simple component. Moreover, since pure standards of TiN and TiB_2 compounds are not accurately produced, the best prepared samples were TiN sample with 54% nitrogen and 46% titanium with no boron detected and a sample as close as possible to TiB_2 with 58% boron, 34% titanium and 8% nitrogen (atomic concentrations). The maximum of intensity is at 456.7 eV for TiNO/TiN and at 454.3 eV for TiB_2.

For the lowest duty cycles and up to *dc* = 40% of *P*, curve fitting of Ti 2p and B 1s peaks gives rise to signals corresponding to Ti-B bonds with TiB_2 peak at 454 eV and 187 eV as shown in Fig. 2a and 2c. As expected, a significant contribution of the film oxidation is measured from Ti-O and B-O bonds with TiO_2 peaks at 458 and 464 eV ($2p^{1/2}$ and $2p^{3/2}$ signals in Fig. 2a), and also with BO peak at 192 eV (Fig. 2c). As duty cycle increases (*dc* = 60% of *P* and higher), TiB_2 contribution recorded from Ti 2p and B 1s peaks reduces and vanishes for a constant supply of nitrogen. Similarly, the BN peak from N 1s (398 eV) and B 1s (190 eV) becomes more and more intense as well as the TiN peak at 396 eV (Fig. 2b). The film oxidation still remains for any duty cycle but it mainly originates from Ti signals (high reactivity of this metal towards oxygen) with a significant reduction of B-O and N-O bonds influence as shown with NO and BO peaks at 400 eV (Fig 2b) and 192 eV (Fig. 2c). As expected, increasing the duty cycle from 0 to 100% of *P* favors the amount of Ti-N and B-N bonds, whereas that of Ti-B bonds decreases without completely preventing the film oxidation due to the high reactivity between titanium and oxygen.

[Ti], [B] and [N] atomic concentrations in the films as a function of duty cycle (neglecting the oxygen amount due to surface oxidation, mainly) were determined from Ti 2p, N 1s and B 1s signals (Fig. 3).

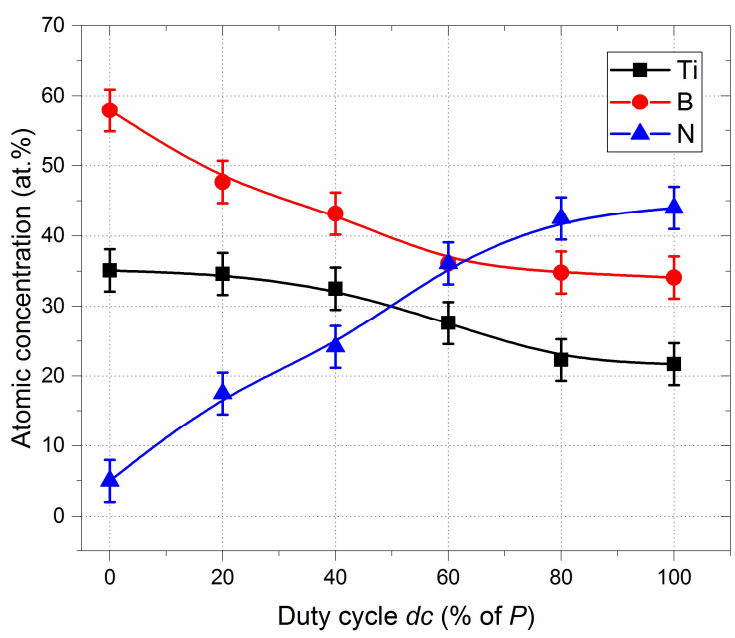

Figure 3. [Ti], [B] and [N] atomic concentrations *vs*. duty cycle *dc* obtained from XPS measurements.

These three element concentrations exhibit a continuous and smooth variation as the nitrogen injection time becomes longer. B and N concentrations show a reverse evolution, while the Ti one slightly reduces (note that concentrations have been determined assuming homogeneous compositions through the film thickness, which is not completely relevant and induces an assumed inaccuracy of ±3 at.% for the chemical concentration). Without nitrogen pulsing (dc = 0% of P), the [B]/[Ti] atomic concentration ratio is close to 1.8. This is lower than the stoichiometric TiB_2 compound due to oxygen occurrence (more than 10 at.%) and a few at.% of nitrogen. When nitrogen is constantly injected (*dc* = 100% of *P*), nitrogen-rich Ti-B-N films are prepared with [N] higher than 44 at.% and [B] around 35 at.%. It is also worth noting that for duty cycles higher than 60% of *P*, the three element concentrations tend to stabilize. The reverse evolution of nitrogen and boron contents *vs.* nitrogen supply agrees with results previously reported by Pierson *et al.* [37] and Han *et al.* [38], who also sputter-deposited Ti-B-N films from a TiB_2 target in Ar + N_2 atmosphere. The authors also noticed the same kind of saturation for Ti, B and N atomic concentrations as the nitrogen flow rate increased (stabilization of the concentrations for nitrogen injections depending on the operating conditions).

The composition of the films is plotted within the Ti-B-N ternary phase diagram (Fig. 4).

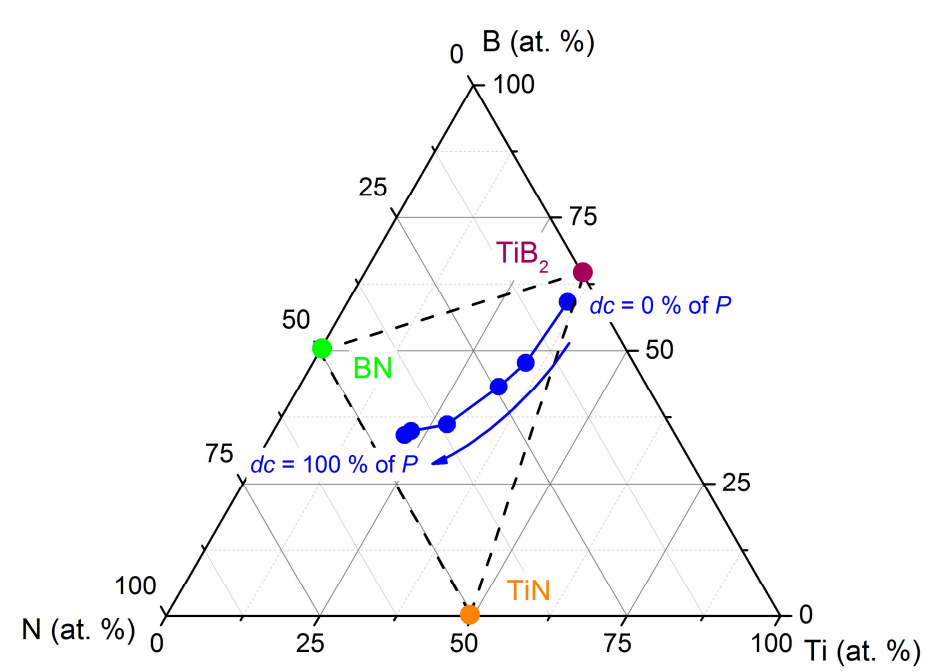

Figure 4. The composition of Ti-B-N films (blue symbols) sputter-deposited by pulsing the nitrogen gas from *dc* = 0 to 100% of the pulsing period *P* = 10 s within a ternary phase diagram. Positions of TiB_2, TiN and BN stoichiometric compounds are indicated as well as quasi-binary tie lines between the individual compounds (dashed lines).

TiB_2, TiN and BN stoichiometric compounds are also indicated as well as quasi-binary tie lines between these individual compounds (dashed lines). Nitrogen pulsing does not produce a chemical composition evolution along the quasi-binary TiN-TiB_2 line as reported for Ti-B-N films prepared by PACVD [39]. It rather moves away from such a line as the duty cycle increases with a BN-enrichment of the films as the nitrogen supply tends to be constant. The same trend has ever been reported by others [40, 41] giving rise to a comparable saturation of nitrogen content in the Ti-B-N films, even by sputtering a TiB_2 target in a pure nitrogen atmosphere. At first and as proposed by Mayrhofer *et al.* [42], we may suggest the formation of a composite structure composed of TiN and TiB_2 nano-crystals randomly distributed in the film, and embedded into a disordered and

amorphous a-BN_x compound. Assuming this nanocrystalline Ti-B-N structure, the corresponding phase proportions (mole fractions) are 42% TiN, 10% TiB_2 and 48% BN in the equilibrium phase diagram for Ti-B-N films prepared with *dc* = 100% of *P*. As expected, reducing the duty cycle leads to lower contents of TiN and BN phases (e.g., for *dc* = 40% of *P*, phase proportions in mole fractions are to 28% TiN, 53% TiB_2 and 19% BN). It is also worth noticing that using a short injection time of nitrogen (*dc* = 20% of *P*) leads to a significant incorporation of N in Ti-B-N films due to the high reactivity of nitrogen towards titanium and boron elements.

Occurrence of chemical bonds can be brought to the fore from FTIR analyses, especially for light elements like B and N. Figure 5 shows FTIR spectra recorded for Ti-B-N films deposited on (100) silicon and for various duty cycles. No clear signals are recorded for duty cycles lower than 45% of *P*. Some peaks appear as the nitrogen injection time increases and they become more significant when duty cycle exceeds 55% of *P*. A broad asymmetric band appears close to 1390 cm^{-1} and clearly develops as *dc* reaches 90% of *P*, which is mainly assigned to the characteristic absorption of hexagonal BN (in-plane B-N bond stretching) in Ti-B-N single layer [43, 44].

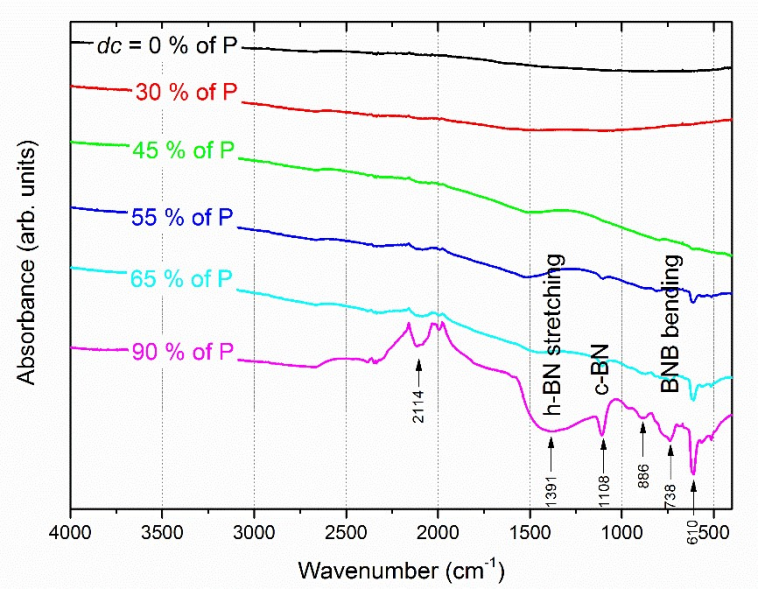

Figure 5. FTIR spectra measured for Ti-B-N films prepared by pulsing the nitrogen gas with an increasing duty cycle from 0 to 90% of the pulsing period *P* = 10 s.

Similarly, a broad and significant signal is measured around 738 cm^{-1} related to the B-N-B bending mode occurring in amorphous boron nitride [37] and a second one is associated with the transverse optical mode of the cubic BN phase at 1108 cm^{-1} [45, 46]. A narrow and intense peak can also be noticed at 610 cm^{-1} with a few weak peaks between 500 and 600 cm^{-1}. This group of signals correspond to Ti-N bonds (typical stretching mode of TiN around 600 cm^{-1} [47]). All these FTIR signals support the formation and increasing amount of B-N and Ti-N bonds for high duty cycles, keeping an amorphous film structure. These results agree with X-ray diffraction analyses where no diffraction peaks due to boron nitride or other phases were detected (not shown here).

3.2. Electrical properties

DC electrical resistivity at room temperature ρ_{300K} of Ti-B-N thin films deposited on glass continuously rises as a function of the duty cycle and spanning more than 6 orders of magnitude as *dc* changes from 0 to 100% of *P* (Fig. 6). Since the nitrogen pulsing period is very short (P = 10 s) and due to deposition rates varying from 9.3 to 14.6 nm min^{-1} (Fig. 1), one can first assume that a random N and B distribution is produced through the film

thickness rather than a multilayered structure, which could influence electrical conductivity, as previously reported for metal/metal oxide coatings [48]. For *dc* lower than 40% of *P*, resistivity is in the range of typical metals, i.e., below 10^{-5} Ω m. Afterwards, Ti-B-N films abruptly become more resistive for duty cycles between 40 and 80% of *P*, and tend to stabilize to a few Ω m as the nitrogen gas is constantly supplied. Carrier mobility μ_{300K} and carrier concentration n_{300K} at 300 K are also both influenced by the nitrogen injection for a similar range of duty cycles. The carrier concentration is over 10^{28} m^{-3} for films prepared with duty cycles lower than 40% of P, which typically corresponds to metallic-like behaviors. It loses several orders of magnitude as duty cycle changes from 60 to 100% of *P* where $n_{300K} = 2.9\times10^{19}$ m^{-3}. Similarly, the carrier mobility exhibits a reverse evolution with μ_{300K} lower than a few 10^{-4} m^2 V^{-1} s^{-1} for the lowest duty cycles, whereas it reaches 2.0×10^{-2} m^2 V^{-1} s^{-1} for $dc = 100\%$ of *P*. As a result, this drop of conductivity is mainly assigned to the strong decrease of the free carrier concentration, which prevails on an enhanced mobility. These significant variations of electronic transport properties of Ti-B-N films correlate with their nitrogen enrichment and thus, with an increasing amount of amorphous BN phase. These results support conclusions previously reported by Rogl [18], who claimed that we may expect a metallic-like behavior for boron-rich compounds, but with an increasing nitrogen content semiconducting to insulating properties develop.

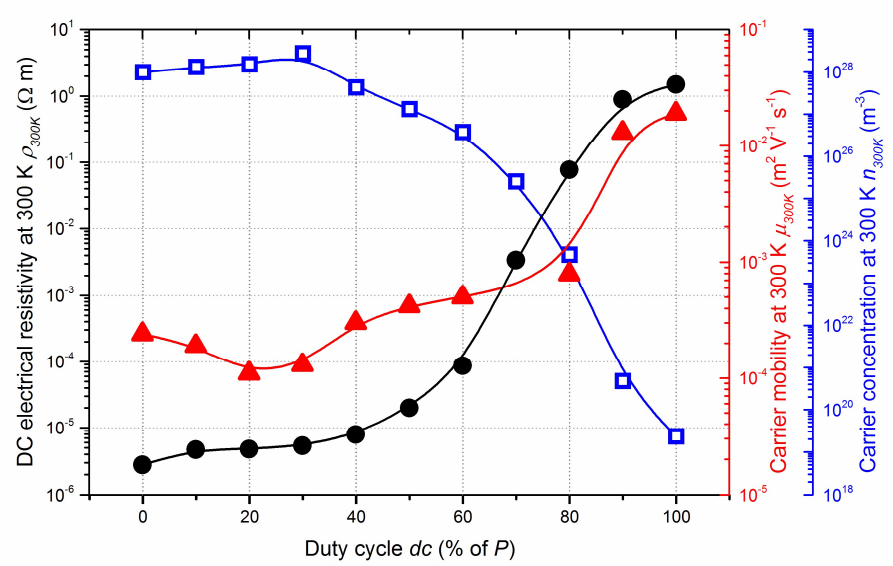

Figure 6. DC electrical resistivity ρ_{300K}, carrier mobility μ_{300K} and carrier concentration n_{300K} measured at room temperature as a function of the duty cycle *dc* of Ti-B-N thin films.

In addition, it is interesting of noting that this abrupt increase of resistivity obtained for duty cycles in-between 40-80% of *P* also corresponds to the transition from absorbent (metallic-like) to transparent (semiconducting-like) Ti-B-N films in the visible region (optical transmittance spectra of Ti-B-N films deposited on glass not shown here).

Resistivity *vs.* temperature also support this gradual metal-to-semiconducting transition as the duty cycle and thus the nitrogen content in Ti-B-N films rises (Fig. 7). A nearly temperature independent resistivity can be noticed for the lowest duty cycles where ρ is kept nearly constant from 30 to 200°C with for example, a negative temperature coefficient of resistance at 300 K (TCR_{300K}) of -8.6×10^{-5} K^{-1} for films prepared without nitrogen pulsing. This is consistent with Pierson *et al.* [49] results, who also reported negative TCR values and the loss of metallic character even for Ti-B-N films prepared with low nitrogen flow rates. Their results also showed a significant increase of TiBN electrical resistance for a given range of nitrogen flow rates corresponding to negative TCRs, which is in some ways similar to the sudden increase of resistivity measured for duty cycles higher than 40% of P (Fig. 6). In our TiBN films, TCR_{300K} becomes even more negative for

dc = 50% of *P* with TCR_{300K} = -3.9×10^{-4} K^{-1} and a further increase of the nitrogen injection time leads to a semiconducting-like behavior with an exponential decrease of the film resistivity as the temperature rises. An Arrhenius plot (electrical conductivity *vs.* reciprocal temperature) gives rise to an activation energy E_a = 12 meV for *dc* = 60% of *P* and reaches 124 meV for a constant supply of the nitrogen flow rate (*dc* = 100% of *P*). This increasing activation energy is connected to the nitrogen-enrichment of Ti-B-N films and so, to the formation of an amorphous and insulating BN phase. However, the highest value of activation energy is quite low compared to typical semiconducting materials, but it remains in the order of magnitude of some nitride or boride semiconductors where the temperature dependent resistivity strongly depends on their composition [50].

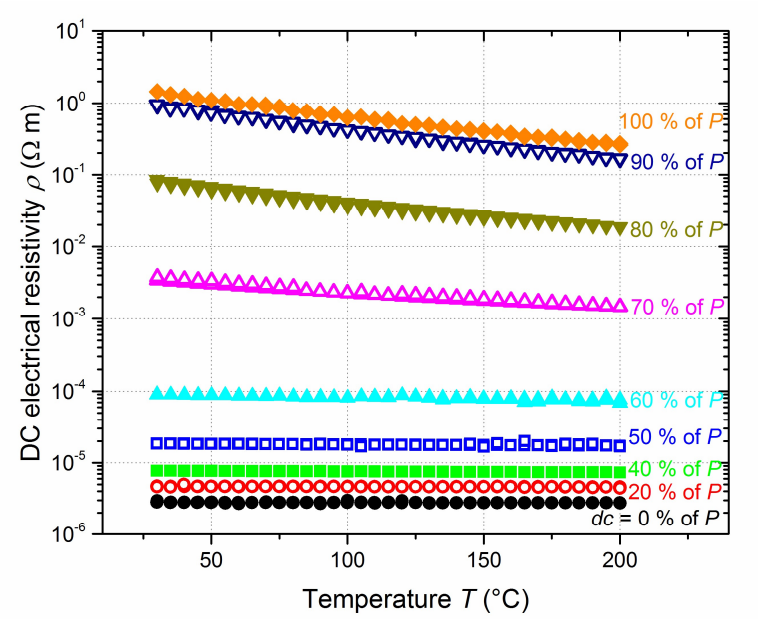

Figure 7. DC electrical resistivity ρ *vs.* temperature T measured on Ti-B-N thin films deposited on glass for various duty cycles (*dc* = 0 to 100% of the constant pulsing period *P* = 10 s).

Our results clearly show that electronic transport characteristics of Ti-B-N films progressively but rapidly change from metallic-to-semiconducting behaviors as a function of the duty cycle, which are directly associated to variations of composition and structure. At first and as frequently modeled for Ti-B-N mechanical properties, we can suppose that films exhibit a nanocomposite structure [39, 42, 51]. The latter is made of nanometric TiN and TiB_2 crystallites (conductive phase) embedded in a disordered BN matrix (insulating medium).

Based-on the sudden change of electrical properties of Ti-B-N films for a given range of duty cycles (Fig. 6) and assuming a nanocomposite structure, a percolation model has been used to describe the evolution of thin film conductivity at 300 K σ_{300K} as a function of 1 - *ndc*, where *ndc* is defined as the normalized duty cycle (Fig. 8). Sputtering conditions with 1 - *ndc* = 0 corresponds to the most N-rich Ti-B-N films (i.e., *dc* = 100% of *P*) and so, the most resistive films. Conductivity abruptly rises when 1-*ndc* reaches 0.4 and afterwards tends to saturate. This σ_{300K} *vs.* 1 - *ndc* evolution typically behaves like a percolation phenomenon. Two electrically different media (insulating amorphous BN matrix and conducting TiN and TiB_2 phases) are mixed in Ti-B-N films. The conducting phase proportion increases while increasing 1 - *ndc*. As a result, the insulating-conducting transition corresponds to the percolation threshold, which can be determined assuming an effective medium theory (EMT) [52]. The percolation theory allows describing the electrical conductivity of a composite medium before and after the percolation threshold ϕ_c through the following equations [53]:

$$\sigma = \sigma_i \left(\frac{\phi_c - \phi}{\phi_c}\right)^{-s}, \quad (1)$$

before the percolation threshold (i.e., $\phi < \phi_c$), where $\sigma = \sigma_{300K}$ is the DC electrical conductivity at 300 K (S m^{-1}), σ_i the DC electrical conductivity of the insulating medium (S m^{-1}), $\phi = 1 - ndc$ the conducting phase ratio (arb. units), and s the critical exponent in the insulating region.

$$\sigma = \sigma_c \left(\frac{\phi - \phi_c}{1 - \phi_c}\right)^{t}, \quad (2)$$

after the percolation threshold (i.e., $\phi > \phi_c$), where σ_c is the DC electrical conductivity of the conducting phase (S m^{-1}), and t the critical exponent in the conducting region.

For the full range of conducting phase ratios ϕ, a phenomenological relationship can be used as suggested by McLachlan *et al.* [54]:

$$(1-\phi)\left(\frac{\sigma_i^{\frac{1}{s}} - \sigma^{\frac{1}{s}}}{\sigma_i^{\frac{1}{s}} - A\sigma^{\frac{1}{s}}}\right) + \phi\left(\frac{\sigma_c^{\frac{1}{t}} - \sigma^{\frac{1}{t}}}{\sigma_c^{\frac{1}{t}} - A\sigma^{\frac{1}{t}}}\right) = 0, \quad (3)$$

with $A = \frac{1-\phi_c}{\phi_c}$.

The best fittings have been performed from these equations as shown in figure 8 (red and green lines for equations (1) and (2), respectively). A percolation threshold $\phi_c = 0.45$ is obtained, which corresponds to dc = 55% of P. From the chemical compositions determined from XPS analyses (Fig. 3), this duty cycle produced comparable B and N concentrations in Ti-B-N films. This result supports Mayrhofer *et al.* who claimed that this range of compositions matches with a film composed of two nanoscale phases (2-3 nm) encapsulated by a high-volume fraction (about 50%) of disordered phase [38, 41].

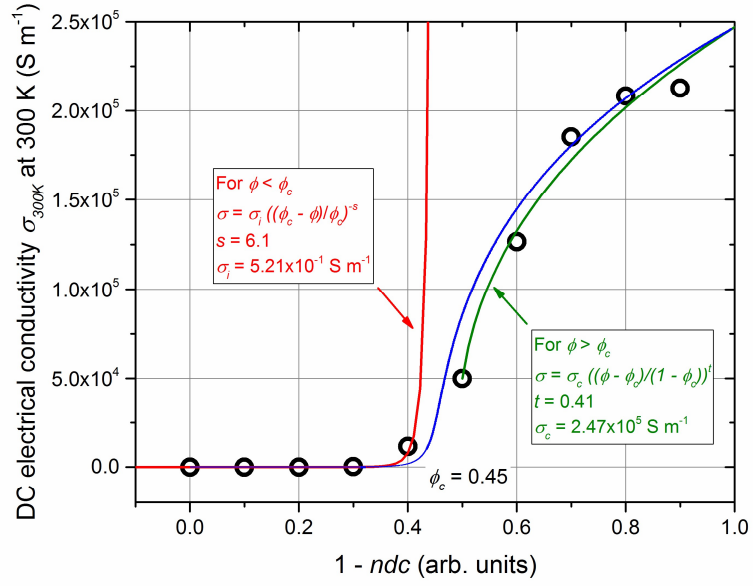

Figure 8. DC electrical conductivity at room temperature σ_{300K} *vs.* $\phi = 1 - ndc$ for Ti-B-N thin films (*ndc* is the normalized duty cycle). Red and green lines are related to the conductivity calculated from the fitting before (equation (1)) and after (equation (2)) the percolation threshold. The blue line is the best fit obtained from equation (3).

It should also be pointed out that from the experimental data at $\phi = 1$, conductivity of the conducting phase is $\sigma_c = 2.47\times10^5$ S m^{-1}. This value is lower than that of single TiN and TiB_2 films ($\sigma_{TiN} = 1.85\times10^6$ S m^{-1} [55] and $\sigma_{TiB2} = 3.52\times10^6$ S m^{-1} [56]) since the conducting phase certainly contains defects and is made of small grains (a few nm), but it remains in the order of magnitude of metallic materials. About the insulating medium, results of the

fits give $\sigma_i = 5.21\times10^{-1}$ S m^{-1}. This value is higher than conductivities usually reported for BN compounds (σ is below 10^{-6} S m^{-1} for pure c-BN at room temperature [57]). This difference is understandable since electronic transport properties of BN strongly depend on crystallinity, preparation method, nature and type of doping [57]. In our Ti-B-N films, the insulating matrix certainly contains a significant amount of defects and Ti, which favor mobility and concentration of free carriers and thus enhance the overall conductivity.

Critical exponents s and t are also of interest, and universal values in-between s_{un} = 0.7-1 and t_{un} = 1.6-2 are commonly reported for three dimensional systems with an inverse Swiss cheese model [52]. For our Ti-B-N films, fittings from experimental data lead to s = 6.1 and t = 0.41, which are significantly different compared to universal values. These discrepancies can be assigned to an inhomogeneous structure of the films (percolation theory is based-on perfect spherical particles for both insulating and conducting media). Sputtering deposition at room temperature often leads to columnar architectures [58] and RGPP may produce periodic multilayers [59]. As a result, our Ti-B-N films can be considered as an anisotropic system affecting the percolation law since the assumed homogeneity and sphericity of media are not fully established. However, fitting with equation (3) and using parameters obtained from each region allows a reliable description of the electrical conductivity of Ti-B-N films for the full range of duty cycles (blue line in Fig. 8). This two-exponent phenomenological percolation equation can be valuably used for assessing the complex DC electrical conductivity of Ti-B-N films exhibiting reverse B and N concentrations.

4. Conclusions

Ti-B-N thin films 300 nm thick are sputter-deposited by RF reactive sputtering. A TiB_2 target is sputtered in a reactive atmosphere composed of Ar and N_2 gases. The reactive gas pulsing process (RGPP) is implemented to inject the nitrogen gas with a constant pulsing period P = 10 s. A systematic variation of the duty cycle dc (t_{ON} injection time) is carried out in order to tune the chemical composition of the films. A nitrogen-enrichment is obtained as the dc gradually increases from 0 to 100% of P. In the same way, the boron concentration is inversely reduced keeping a nearly constant Ti content. It is also shown that increasing the nitrogen injection time favors the B-N bonds occurrence in the films with a phase proportion close to 48% of BN (mole fraction) when the nitrogen is constantly supplied (dc = 100% of P).

For duty cycles in-between 40-80% of P, electronic transport properties measured at room temperature significantly change with a resistivity enhancement of 4 orders of magnitude, while carrier mobility and concentration correspondingly change for the same range of dc. A regular but rapid transition from a metallic to semiconducting-like behavior is clearly brought to the fore as a function of the duty cycle, which is supported from resistivity *vs.* temperature measurements. Assuming a nanocomposite structure in Ti-B-N films made of nanometric TiN and TiB_2 crystallites (conductive phase) embedded in a disordered BN matrix (insulating medium), a percolation model well describes the tunable films conductivity as a function of the nitrogen injection.

These results demonstrate that the nanocomposite structure successfully proposed for mechanical properties and wear resistance of Ti-B-N films, can also be applied to well describe the electrical properties of such films as a function of B and N concentrations. They also show that RGPP technique is a suitable approach to adjust electronic transport properties by means of a simple and easy change a pulsing parameter. A further incorporation of nitrogen in the films would be relevant to extend even more the multiphase nanostructuring growth.

Author Contributions: Conceptualization, data curation, C. Sakkas; methodology, software, J.M. Cote; formal analysis, validation, J. Gavoille; formal analysis, validation, J.Y. Rauch; formal analysis, validation, P.H. Cornuault; data curation, investigation, A. Krystianiak; formal analysis, validation,

O. Heintz; writing—review and editing, funding acquisition, N. Martin. All authors have read and agreed to the published version of the manuscript. All authors have read and agreed to the published version of the manuscript.

Funding: Please add: This research was partially funded by Fonds Européen de Développement Régional – FEDER, grant number CTE 6059 in the framework of the TOOLEXPERT Interreg V project.

Institutional Review Board Statement: Not applicable.

Informed Consent Statement: Not applicable.

Data Availability Statement: All data are presented in the current manuscript.

Acknowledgments: This work has been supported by the Région Bourgogne Franche-Comté and by EIPHI Graduate School (Contract 'ANR-17-EURE-0002').

Conflicts of Interest: The authors declare no conflict of interest. The funders had no role in the design of the study; in the collection, analyses, or interpretation of data; in the writing of the manuscript; or in the decision to publish the results.

References

1. McManus-Driscoll, J.L.; Zerrer, P.; Wang, H.; Yang, H.; Yoon, J.; Fouchet, A.; Yu, R.; Blamire, M.G.; Jia, Q. Strain and spontaneous phase ordering in vertical nanocomposite heteroepitaxial thin films. *Nature Mater.* **2008**, 7, 314-320. https://doi.org/10.1038/nmat2124
2. Chen, A.; Bi, Z.; Jia, Q.; MacManus-Driscoll, J.L.; Wang, H. Microstructure, vertical strain control and tunable functionality in self-assembled vertically aligned nanocomposite thin films. *Acta Mater.* **2013**, 61(8), 2783-2792. https://doi.org/10.1016/j.actamat.2012.09.072
3. Wu, J.F.; Yu, L.H.; Hu, H.B.; Asempah, I.; Xu, J.H. Structural, mechanical and tribological properties of NbCN-Ag nanocomposite films deposited by reactive magnetron sputtering. *Coatings* **2018**, 8(2), 50-15. https://doi.org/10.3390/coatings8020050
4. Lopez, D.A.S.; Chagas, L.G.; Batista, A.D.; Guaita, M.G.D.; Amorin, L.H.C.; Da Silva, P.R.C.; Yamashini, G.; Zaia, D.A.M.; De Santana, H.; Urbano, A. Effect of RF magnetron sputtering parameters on the optimization of the discharge capacity of ternary lithium oxide thin films. *J. Mater. Sci.* **2021**, 32, 17462-17472. https://doi.org/10.21203/rs.3.rs-363697/v1
5. Txintxurreta, J.; G-Berasategui, E.; Ortiz, R.; Hernandez, O.; Mendizabal, L.; Barriga, J. Indium oxide thin film deposition by magnetron sputtering at room temperature for the manufacturing of efficient transparent heaters. *Coatings* **2021**, 11, 92-14. https://doi.org/10.3390/coatings11010092
6. Saikumar, A.K.; Sundaresh, S.; Nehate, S.D.; Sundaram, K.B. Properties of RF magnetron sputtered copper gallium oxide ($CuGa_2O_4$) thin films. *Coatings* **2021**, 11, 921-11. https://doi.org/10.3390/coatings11080921
7. Rebholz, C.; Leyland, A.; Schneider, J.M.; Voevodin, A.A.; Matthews, A. Structure, hardness and mechanical properties of magnetron-sputtered titanium-aluminium boride thin films. *Surf. Coat. Technol.* **1999**, 120, 412-417. https://doi.org/10.1016/s0257-8972(99)00490-9
8. Minemoto, T.; Negami, T.; Nishiwaki, S.; Takakura, H.; Hamakawa, Y. Preparation of $Zn_{1-x}Mg_xO$ films by radio frequency magnetron sputtering. *Thin Solid Films* **2000**, 372, 173-176. https://doi.org/10.1016/s0040-6090(00)01009-9
9. Greczynski, G.; Lu, J.; Jensen, J.; Bolz, S.; Kolker, W.; Schiffers, C.; Lemmer, O.; Greene, J.E.; Hultman, L. A review of metal-ion-flux-controlled growth of metastable TiAlN by HIPIMS/DCMS co-sputtering. *Surf. Coat. Technol.* **2014**, 257, 15-25. https://doi.org/10.1016/j.surfcoat.2014.01.055
10. Palmquist, J.P.; Birch, J.; Jansson, U. Deposition of epitaxial ternary metal carbide films. *Thin Solid Films* **2002**, 405, 122-128. https://doi.org/10.1016/s0040-6090(01)01766-7
11. Glynn, C.; Aureau, D.; Collins, G.; O'Hanlon, S.; Etcheberry, A.; O'Dwyer, C. Solution processable broadband transparent mixed metal oxide nanofilm optical coatings via substrate diffusion doping. *Nanoscale* **2015**, 7, 20227-20237. https://doi.org/10.1039/c5nr06184a
12. Steinecke, M.; Kiedrowski, K.; Jupé, M.; Ristau, D. Very thick mixture oxide ion beam sputtering films for investigation of nonlinear material properties. *Eur. Phys. J. Appl. Phys.* **2017**, 80, 30301-5. https://doi.org/10.1051/epjap/2017170239
13. Martin, N.; Banakh, O.; Santo, A.M.E.; Springer, S.; Sanjinès, R.; Takadoum, J.; Lévy, F. Correlation between processing and properties of TiO_xN_y thin films sputter deposited by the reactive gas pulsing technique. *Appl. Surf. Sci.* **2001**, 185, 123-133. https://doi.org/10.1016/s0169-4332(01)00774-7
14. Vaz, F.; Cerqueira, P.; Rebouta, L.; Nascimento, S.M.C.; Alves, E.; Goudeau, P.; Rivière, J.P.; Pischow, K.; de Rijk, J. Structural, optical and mechanical properties of coloured TiN_xO_y thin films. *Thin Solid Films* **2004**, 447, 449-454. https://doi.org/10.1016/s0040-6090(03)01123-4

15. Fernandes, A.C.; Carvalho, P.; Vaz, F.; Lancero-Mendez, S.; Machado, A.V.; Parreira, N.M.G.; Pierson, J.F.; Martin, N. Property change in multifunctional TiC_xO_y thin films: Effect of the O/Ti ratio. *Thin Solid Films* **2006**, 515, 866-871. https://doi.org/10.1016/j.tsf.2006.07.047
16. Sanchez-Lopez, J.C.; Abad, M.D.; Carvalho, I.; Galindo, R.E.; Benito, N.; Ribeiro, S.; Henriques, M.; Cavaleiro, A.; Carvalho, S. Influence of silver content on the tribomechanical behavior on Ag-TiCN bioactive coatings. *Surf. Coat. Technol.* **2012**, 206, 2192-2198. https://doi.org/10.1016/j.surfcoat.2011.09.059
17. Ji, A.L.; Ma, L.B.; Liu, C.; Li, C.R.; Cao, Z.X. Synthesis and characterization of superhard aluminum carbonitride thin films. *Diam. Relat. Mater.* **2005**, 14, 1348-1352. https://doi.org/10.1016/j.diamond.2005.01.036
18. Rogl, P. Materials science of ternary metal boron nitrides. *Int. J. Inorg. Mater.* **2001**, 3, 201-209. https://doi.org/10.1016/s1466-6049(01)00009-5
19. Lu, Y.H.; Zhou, Z.F.; Sit, P.; Shen, Y.G.; Li, K.Y.; Chen, H. X-Ray photoelectron spectroscopy characterization of reactively sputtered Ti-B-N thin films. *Surf. Coat. Technol.* **2004**, 187, 98-105. https://doi.org/10.1016/j.surfcoat.2003.11.024
20. Tian, C.X.; Wang, Z.S.; Zou, C.W.; Tang, X.S.; Xie, X.; Lie, S.Q.; Liang, F.; Li, Z.J.; Liu, Y.F.; Su, F.H. Ternary and quaternary TiBN and TiBCN nanocomposite coatings deposited by arc ion plating. *Surf. Coat. Technol.* **2019**, 359, 445-450. https://doi.org/10.1016/j.surfcoat.2018.12.081
21. Lu, Y.H.; Shen, Y.G.; Li, K.Y. Nanostructured two-phase nc-TiN/a-(TiB_2, BN) nanocomposite thin films. *Appl. Surf. Sci.* **2006**, 253, 1631-1638. https://doi.org/10.1016/j.apsusc.2006.02.058
22. Mayrhofer, P.H.; Willmann, H.; Mitterer, C. Recrystallization and grain growth of nanocomposite Ti-B-N coatings. *Thin Solid Films* **2003**, 440, 174-179. https://doi.org/10.1016/s0040-6090(03)00858-7
23. Aoudi, S.M.; Namavar, F.; Gorishnyy, T.Z.; Rohde, S.L. Characterization of TiBN films grown by ion beam assisted deposition. *Surf. Coat. Technol.* **2002**, 160, 145-151. https://doi.org/10.1016/s0257-8972(02)00330-4
24. Andrievski, R.A. Structure and properties of nanostructured boride/nitride materials. *Int. J. Refract. Met. Hard Mater.* **1999**, 17, 153-155. https://doi.org/10.1016/s0263-4368(98)00072-9
25. Mayrhofer, H.; Mitterer, C.; Clemens, H. Self-organized nanostructures in hard ceramic coatings. *Adv. Eng. Mater.* **2005**, 7(12), 1071-1082. https://doi.org/10.1002/adem.200500154
26. Kainz, C.; Schalk, N.; Tkadletz, M.; Mitterer, C.; Czettl, C. The effect of B and C addition on microstructure and mechanical properties of TiN hard coatings grown by chemical vapor deposition. *Thin Solid Films* **2019**, 688, 137283-8. https://doi.org/10.1016/j.tsf.2019.05.002
27. Zhou, S.Y.; Pelenovich, V.O.; Han, B.; Yousaf, M.I.; Yan, S.J.; Tian, C.X.; Fu, D.J. Effects of modulation period on microstructure, mechanical properties of TiBN/TiN nanomultilayered films deposited by multi arc ion plating. *Vacuum* **2016**, 126, 34-40. https://doi.org/10.1016/j.vacuum.2016.01.007
28. Asempah, I.; Xu, J.H.; Yu, L.H.; Luo, H.; Liu, J.L.; Yu, D.; Ding, N. The role of copper incorporation on the microstructure, mechanical and tribological properties of TiBN-Cu films by reactive magnetron sputtering. *J. Alloy. Compd.* **2019**, 801, 112-122. https://doi.org/10.1016/j.jallcom.2019.06.053
29. Cicek, H.; Baran, O.; Demirci, E.E.; Tahmasebian, M.; Totik, Y.; Efeoglu, I. The effect of nitrogen flow rate on TiBN coatings deposited on cold work tool steel. *J. Adhes. Sci. Technol.* **2014**, 28, 1140-1148. https://doi.org/10.1080/01694243.2014.888890
30. Martin, N.; Lintymer, J.; Gavoille, J.; Chappé, J.M.; Sthal, F.; Takadoum, J.; Vaz, F.; Rebouta, L. Reactive sputtering of TiO_xN_y coatings by the reactive gas pulsing process – Part I : pattern and period of pulses. *Surf. Coat. Technol.* **2007**, 201, 7720-7726. https://doi.org/10.1016/j.surfcoat.2007.03.002
31. El Mouatassim, A.; Pac, M.J.; Pailloux, F.; Amiard, G.; Henry, P.; Rousselot, C.; Eydi, D.; Tuilier, M.H.; Cabioc'h, T. On the possibility of synthesizing multilayered coatings in the (Ti, Al)N system by RGPP: A microstructural study, *Surf. Coat. Technol.* **2019**, 374, 845-851. https://doi.org/10.1016/j.surfcoat.2019.06.071
32. Fairley, N.; Fernandez, V.; Richard-Plouet, M.; Guillot-Deudon, C.; Walton, J.; Smith, E.; Flahaut, D.; Greiner, M.; Biesinger, M.; Tougaard, S.; Morgan, D.; Baltrusaitis, J. Systematic and collaborative approach to problem solving using X-ray photoelectron spectroscopy, **2021**, 5, 100112-9. https://doi.org/10.1016/j.apsadv.2021.100112 .
33. Chaleix, L.; Machet, J. Study of the composition and of the mechanical properties of TiBN films obtained by d.c. magnetron sputtering. *Surf. Coat. Technol.* **1997**, 91, 74-82. https://doi.org/10.1016/s0257-8972(96)03139-8
34. Pierson, J.F.; Chapusot, V.; Billard, A.; Alnot, M.; Bauer, P. Characterisation of reactively sputtered of Ti-B-N and Ti-B-O coatings. *Surf. Coat. Technol.* **2002**, 151-152, 526-530. https://doi.org/10.1016/s0257-8972(01)01583-3
35. Holzschuh, H. Deposition of Ti-B-N (single and multilayer) and Zr-B-N coatings by chemical vapor deposition techniques on cutting tools. *Thin Solid Films* **2004**, 469-470, 92-98. https://doi.org/10.1016/j.tsf.2004.08.077
36. Hahn, R.; Tymoszuk, A.; Wojcik, T.; Kirnbauer, A.; Kozak, T.; Capek, J.; Sauer, M.; Foelske, A.; Hunold, O.; Polcik, P.; Mayrhofer, P.H.; Riedl, H. Phase formation and mechanical properties of reactively and non-reactively sputtered Ti-B-N hard coatings. *Surf. Coat. Technol.* **2021**, 420, 127327-11. https://doi.org/10.1016/j.surfcoat.2021.127327
37. Pierson, J.F.; Tomasella, E.; Bauer, P. Reactively sputtered Ti-B-N nanocomposite films: Correlation between structure and optical properties. *Thin Solid Films* **2002**, 408, 26-32. https://doi.org/10.1016/s0040-6090(02)00071-8
38. Han, B.; Neena, D.; Wang, Z.; Kondamareddy, K.K.; Li, N.; Zuo, W.; Yan, S.; Liu, C.; Fu, D. Investigation of structure and mechanical properties of plasma vapor deposited nanocomposite TiBN films. *Plasma Sci. Technol.* **2017**, 19, 045503-9. https://doi.org/10.1088/2058-6272/aa57eb

39. Mayrhofer, P.H.; Stoiber, M. Thermal stability of superhard Ti-B-N coatings. *Surf. Coat. Technol.* **2007**, 201, 6148-6153. https://doi.org/10.1016/j.surfcoat.2006.08.132
40. Lin, J.; Moore, J.J.; Mishra, B.; Pinkas, M.; Sproul, W.D. The structure and mechanical and tribological properties of TiBCN nanocomposite coatings. *Acta Mater.* **2010**, 58, 1554-1564. https://doi.org/10.1016/j.actamat.2009.10.063
41. Karuna Purnapu Rupa, P.; Chakraborti, P.C.; Mishra, S.K. Structure and indentation behavior of nanocomposite Ti-B-N films. *Thin Solid Films* **2014**, 564, 160-169. https://doi.org/10.1016/j.tsf.2014.05.051
42. Mayrhofer, P.H.; Mitterer, C.; Wen, J.G.; Petrov, I.; Greene, J.E. Thermally induced self-hardening of nanocrystalline Ti-B-N thin films. *J. Appl. Phys.* **2006**, 100, 044301-7. https://doi.org/10.1063/1.2222406
43. Chu, K.; Shen, Y.G. Mechanical and tribological properties of nanostructured TiN/TiBN multilayer films. *Wear* **2008**, 265 516-524. https://doi.org/10.1016/j.wear.2007.11.021
44. Tsai, P.C. The deposition of characterization of BCN films by cathodic arc plasma evaporation. *Surf. Coat. Technol.* **2007**, 201 5108-5113. https://doi.org/10.1016/j.surfcoat.2006.07.119
45. Kurooka, S.; Ikeda, T.; Kohama, K.; Tanaka, T.; Tanaka, A. Formation and characterization of BN films with Ti added. *Surf. Coat. Technol.* **2003**, 166, 111-116. https://doi.org/10.1016/s0257-8972(02)00823-x
46. Moreno, H.; Caicedo, J.C.; Amaya, C.; Munoz-Saldana, J.; Yate, L.; Esteve, J.; Prieto, P. Enhancement of surface mechanical properties by using TiN/$[BCN/BN]_n$/c-BN multilayer system. *Appl. Surf. Sci.* **2010**, 257, 1098-11104. https://doi.org/10.1016/j.apsusc.2010.08.024
47. Sedira, S.; Achour, S.; Avci, A.; Eskizeybek, V. Physical deposition of carbon doped titanium nitride film by DC magnetron sputtering for metallic implant coating use. *Appl. Surf. Sci.* **2014**, 295, 81-85. https://doi.org/10.1016/j.apsusc.2014.01.010
48. Cacucci, A.; Tsiaoussi, I.; Potin, V.; Imhoff, L.; Martin, N.; Nyberg, T. The interdependence of structural and electrical properties in TiO_2/TiO/Ti periodic multilayers. *Acta Mater.* **2013**, 61, 4215-4225. http://dx.doi.org/10.1016/j.actamat.2013.03.047
49. Pierson, J.F.; Bertran, F.; Bauer, J.P.; Jolly, J. Structural and electrical properties of sputtered titanium boronitride films. *Surf. Coat. Technol.* **2001**, 142-144, 906-910. https://doi.org/10.1016/s0257-8972(01)01124-0
50. Wang, C.C.; Akbar, S.A.; Chen, W.; Patton, V.D. Electrical properties of high-temperature oxides, borides, carbides and nitrides. *J. Mater. Sci.* **1995**, 30, 1627-1641. https://doi.org/10.1007/bf00351591
51. Mitterer, C.; Mayrhofer, P.H.; Beschliesser, M.; Losbichler, P.; Warbichler, P.; Hover, F.; Gibson, P.N.; Gissler, W.; Hruby, H.; Musil, J.; Vlcek, J. Microstructure and properties of nancomposite Ti-B-N and Ti-B-C coatings. *Surf. Coat. Technol.* **1999**, 120-121, 405-411. https://doi.org/10.1016/s0257-8972(99)00489-2
52. Nan, C.W. Physics of inhomogeneous inorganic materials. *Progr. Mater. Sci.* **1993**, 37, 1-116. https://doi.org/10.1016/0079-6425(93)90004-5
53. Fabreguette, F.; Maglione, M.; Imhoff, L.; Domenichini, B.; Marco de Lucas, M.C.; Sibillot, P.; Bourgeois, S.; Sacilotti, M. Conductimetry and impedance spectroscopy study of low pressure metal organic chemical vapor deposition TiN_xO_y films as a function of the growth temperature: A percolation approach. *Appl. Surf. Sci.* **2001**, 175-176, 574-578. https://doi.org/10.1016/s0169-4332(01)00121-0
54. McLachlan, D.S.; Cai, K.; Sauti, G. AC and DC conductivity-based microstructural characterization. *Int. J. Refract. Met. Hard Mater.* **2001**, 19, 437-445. https://doi.org/10.1016/s0263-4368(01)00024-5
55. Liang, H.; Xu, J.; Zhou, D.; Sun, X.; Chu, S.; Bai, Y. Thickness dependent microstructural and electrical properties of TiN thin films prepared by DC reactive magnetron sputtering. *Ceram. Int.* **2016**, 42, 2642-2647. https://doi.org/10.1016/j.ceramint.2015.10.070
56. Raman, M.; Wang, C.C.; Chen, W.; Akbar, S.A. Electrical resistivity of titanium diboride and zirconium diboride. *J. Am. Ceram. Soc.* **1995**, 78(5), 1380-1382. https://doi.org/10.1111/j.1151-2916.1995.tb08498.x
57. Zhang, X.W. Doping and electrical properties of cubic boron nitride thin films: A critical review. *Thin Solid Films* **2013**, 544, 2-12. https://doi.org/10.1016/j.tsf.2013.07.001
58. Anders, A. A structure zone diagram including plasma-based deposition and ion etching. *Thin Solid Films* **2010**, 518, 4087-4090. https://doi.org/10.1016/j.tsf.2009.10.145
59. Zaoui, M.; Bourceret, A.; Gaillard, Y.; Giljean, S.; Rousselot, C.; Pac, M.J.; Richard, F. Relation between hardness of (Ti, Al)N based multilayered coatings and periods of their stacking. *Acta Polytech.* **2020**, 27, 79-83. https://doi.org/10.14311/app.2020.27.0079